CHAPTER 5

SUITABILITY OF THE PRESENT CFD MODEL

To check the suitability and find out the behavior of the present model, the model is first used to investigate the transport phenomena of gas diffusion over both flat and non-planar terrain. Comparison of simulation results and analytical solution in the simple case of gas diffusion over flat terrain is discussed in section 5.1. Next, the model is used to simulate and compare with published results of tracer gas dispersion over an isolated hill from wind tunnel experiment.

5.1 Comparison with analytical results of a transport phenomena model for flat terrain

In the system shown in Figure 5.1, a stream of fluid (of chemical species B) in laminar motion has a uniform velocity u_0. At some point in the stream species A is continuously injected in a small amount Q grams sec^{-1}. This amount is assumed to be small enough so that mass average velocity will not deviate appreciably from u_0. Species A is swept downstream (in the z-direction), and at the same time it diffuses both axially and radially (at steady state).

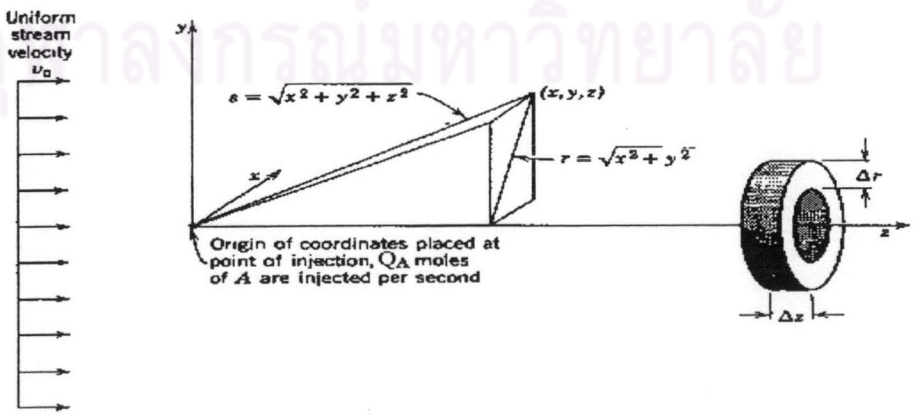

Figure 5.1 Diffusion from a point source in a constant-velocity stream

A mass balance on species A over the cylindrical ring in Figure 5.1, as described in Problem 17.k (R. Byron Bird et al., 1960), was carried out to derive the equation of continuity of A, which is solved to give the analytical solution at steady state below. Here ρ and D_{AB} are assumed to be constant.:

$$C_A = \frac{Q}{4\pi D_{AB} S} \exp[(-u_0 / 2D_{AB})(s - z)] \qquad (5.1)$$

Here C_A = Concentration of A (g/cm^3)

D_{AB} = Diffusion coefficient (cm^2/s)

Q = Emission rate (g/s)

u_o = Uniform velocity (cm/s)

$S = \sqrt{x^2 + y^2 + z^2}$

In this section, the simulation results obtained from the present model will be substantiated against the above analytical solution. The relevant parameters for the analytical solution and simulation are listed in Table 5.1

Table 5.1 Parameters of the transport phenomena and present models

Transport phenomena model	
Diffusion coefficient (D_{AB})	0.25 cm^2/s
Source height	5.7 m.
Uniform velocity (u_0)	2 cm/s
Emission Rate	0.01262 g/s
CFD model	
Number of grid points in the x, y and z directions	66 x 41 x 50
Grid size ($\Delta x, \Delta y, \Delta z$)	25, 25, 25 cm.
Horizontal diffusion coefficient (K_H)	0.25 cm^2/s
Vertical diffusion coefficient (K_v)	0.25 cm^2/s
Node position of source height	$y = 24$
Velocity at source height (u_0)	2 cm/s
Emission rate	0.01262 g/s
Reynolds number	1000
Exponent (n) of the power law	0.000000001
Integration step size (Δt)	0.5 sec

The calculated wind velocity profile is shown in Figure 5.2. The relative concentration along the z-axis (downwind distance) at the source height, 25 cm. above the source height and 25 cm. below the source height, are shown in Figures 5.3 to 5.5.

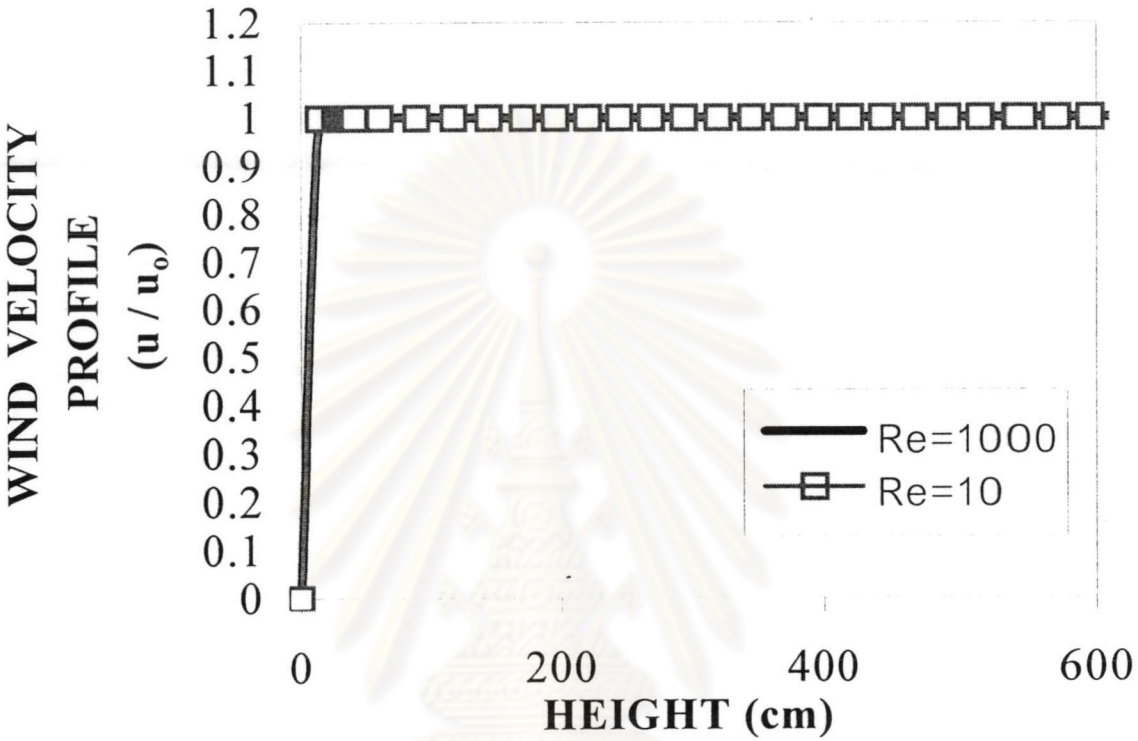

Figure 5.2 Wind velocity profile at x = 25 cm and z = 300 cm from the origin used in the model

Since the wind velocity profile is estimated using the power law, it depends only on the exponent of the power law and not on the Navier-Stokes equation or Reynolds number. Therefore, in Figure 5.2, the calculated wind velocity approximately assumes a flat profile with respect to height and is independent of the Reynolds number. At the source height, the calculated relative concentrations at various downwind distances agree well with the analytical solution, as shown in Figure 5.3. But at 25 cm. below and above the source height, the calculated downwind relative concentrations are over-predicted within the first 0-6 m. downwind of the point source but correctly approach the analytical solution. It is found that the simulated effective plume width is slightly wider than that of the analytical solution. In addition, at a

nearby position directly above or below the point source, the relative concentration will approach zero in the case of the analytical solution. However, in the case of the simulation results, the concentration can not converge to a numerical value much less than the average concentrations of the surrounding node points, which results from the limitation of the finite-difference technique.

In practice the present CFD model is intended for use to predict the atmospheric dispersion of air pollutant over a wide area (long distance downwind), so the observed discrepancy near the point source should not pose a serious problem. On the other hand, if we really need to reduce this discrepancy, then a sufficiently small grid size must be adopted. This however will greatly increase both the required computer memory and the computational time.

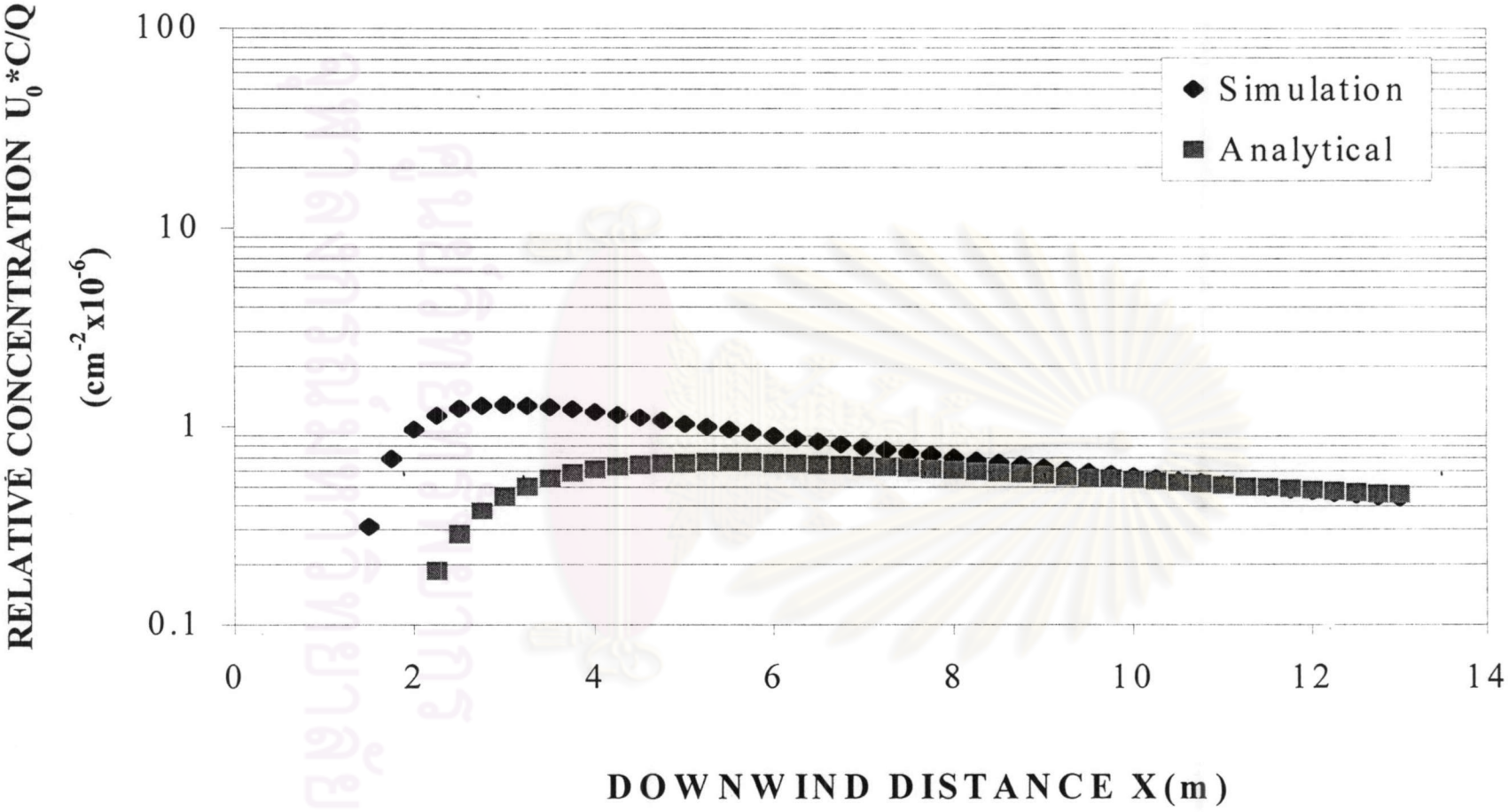

Figure 5.3 Downwind relative concentration of the tracer at the point source height

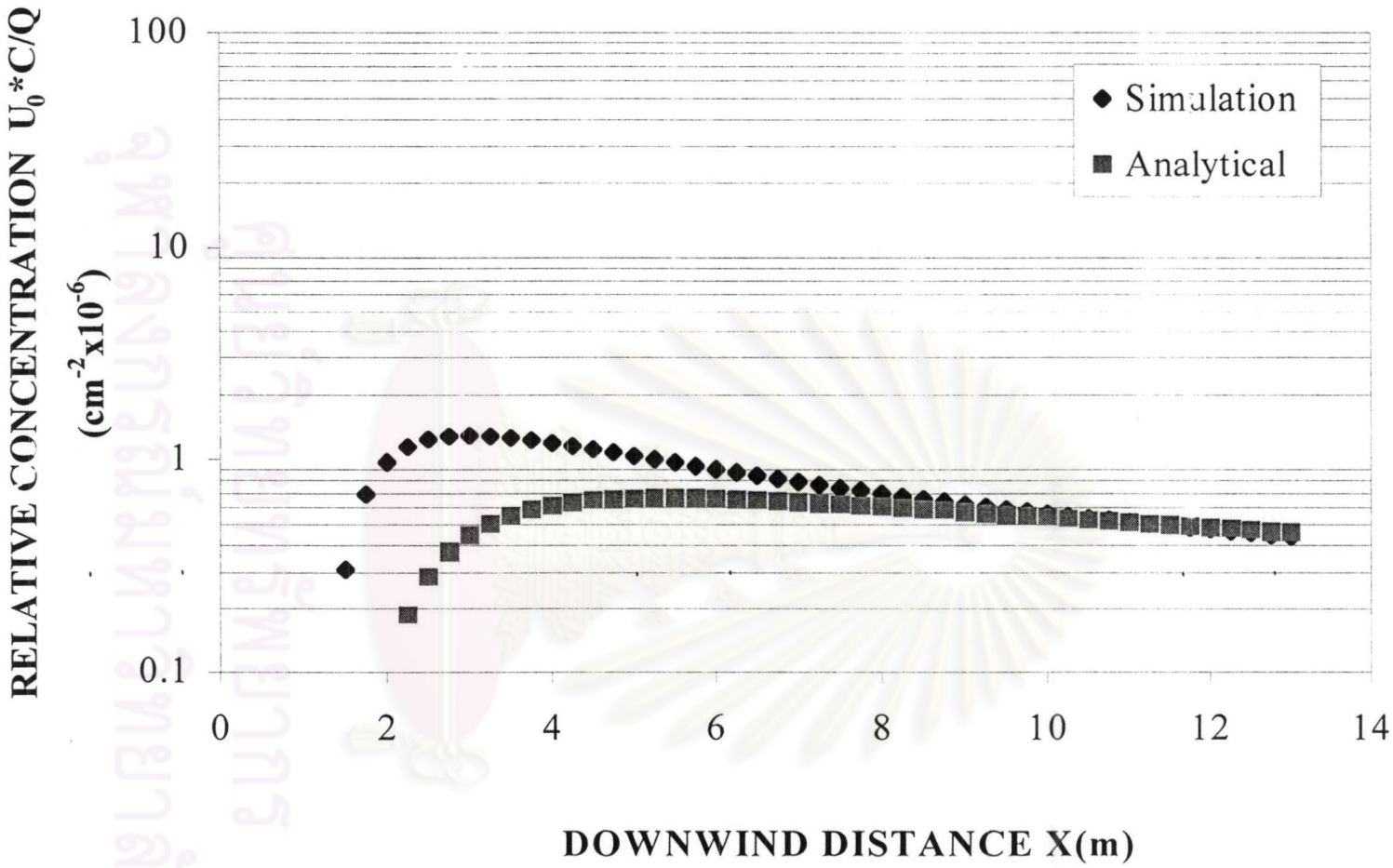

Figure 5. 4 Downwind relative concentration at 25 cm. above the point source height

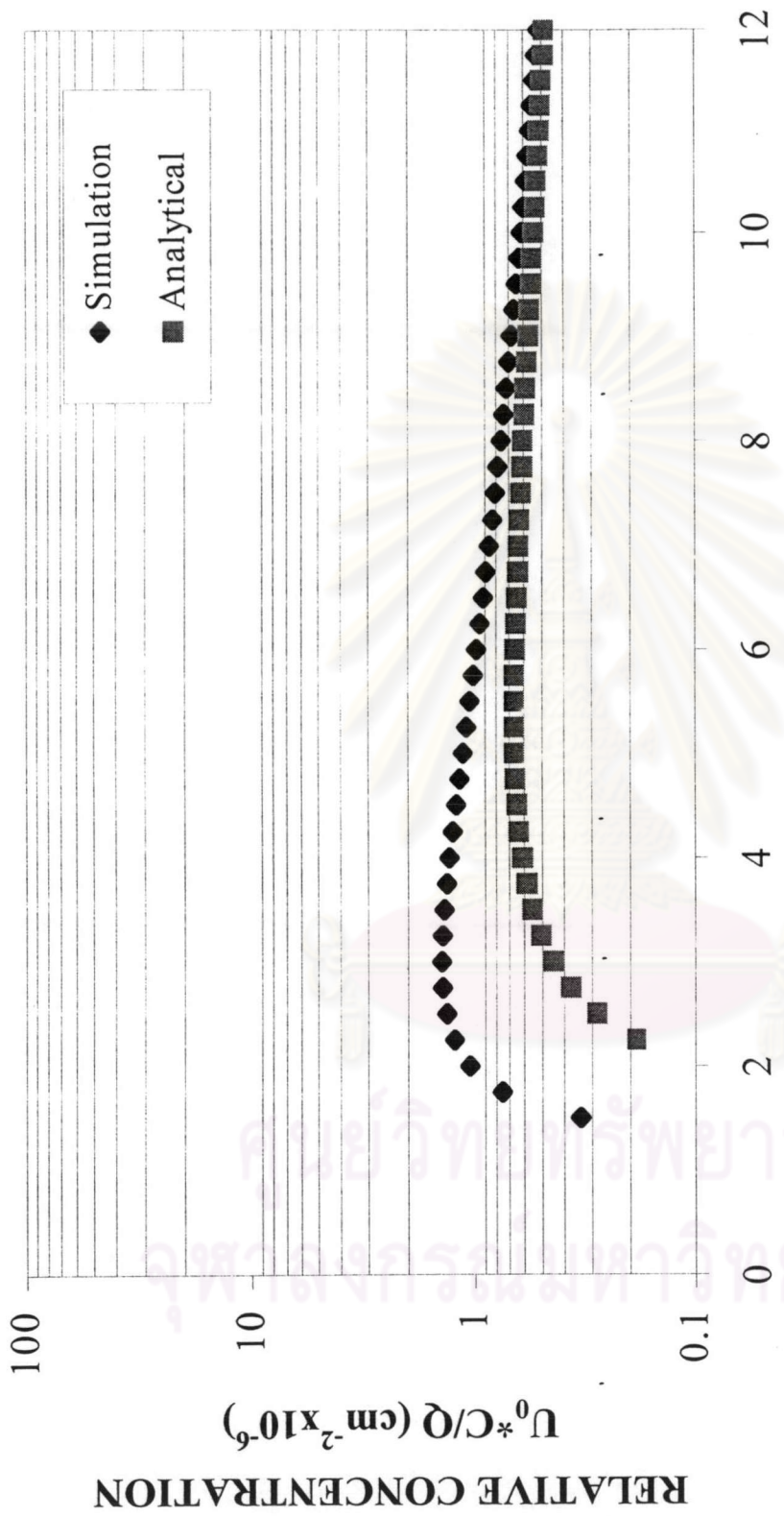

Figure 5. 5 Downwind relative concentrations at 25 cm. below the point source height.

5.2 Comparison with wind-tunnel experiments over non-planar terrain

In this section, the simulation results are compared with wind tunnel experimental results obtained by R. Ohba, et.al. (1990) published in Atmospheric Environment Journal. In their experiment, a tracer gas (either SF_6 or $CBrF_3$) was released upwind of a miniaturized hill modeled after Steptoe Butte Hill, Washington State, and under neutral and stable conditions. The rationale for choosing the wind tunnel experiment is that detailed results of the experiment are available for the air pollutant dispersion under stable condition, which suits the model limitation. In addition, constant wind direction and speed are used during the experimental period. A topographical map of Steptoe Butte area as represented by the wind-tunnel model is illustrated in Figure 5.6. In this study, the 15-min.-averaged ground-level concentration of SF_6 during the third quarter of the first hour in the case of stable atmospheric stability for wind directions of 192 and 228 degrees from the north is compared. According to limitation of the finite-difference model, the concentration at 10 m. above the ground is used to represent the ground-level concentration.

Table 5.2 Model parameters and conditions of wind tunnel experiments

Wind tunnel experiment	
Stability condition	Stable
Source height (equivalent height)	115 m.
Wind velocity at source height	4 m/s
Emission rate from point source	0.631 g/s
Time interval of averaging concentration	30-45 min from start
Simulation calculation	
Number of grid points in the x, y and z directions	29 x 51 x 26
Grid size ($\Delta x, \Delta y, \Delta z$)	200, 20, 200 m.
Velocity at source height (u_0)	4 m/s
Emission rate from point source	0.631 g/s
Integration step size(Δt)	1.0 sec.

Model parameters, including the exponent of the power law, horizontal and vertical dispersion coefficients, and Reynolds number are varied to fit the

calculated concentration to the experimental results. The suitable parameters for this case are listed in Table 5.3.

Table 5.3 The suitable parameters for tracer dispersion over an isolated hill under stable atmospheric condition

Simulation parameters	
The exponents of power law (Pow)	0.55
Horizontal dispersion coefficient (K_H)	200 (m^2/s)
Vertical dispersion coefficient (K_V)	1 (m^2/s)
Reynolds number (Re)	1000

The calculated wind velocity profile and the downwind relative concentrations at 10 m above ground level for two wind directions of 192 and 228 degrees from N, respectively, are compared with the wind tunnel experiments in Figure 5.6 to 5.8.

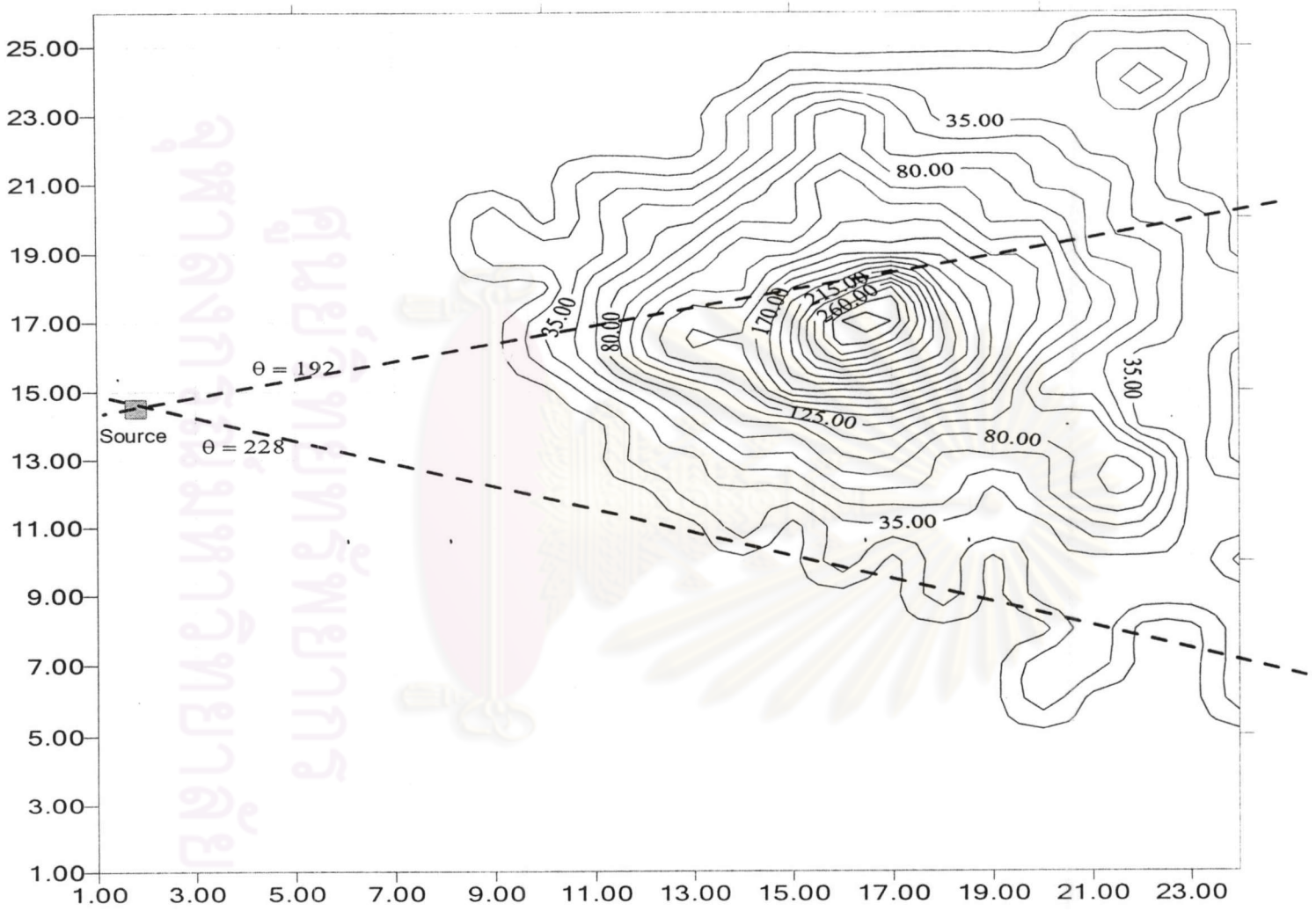

Figure 5.6 A topographical map of the wind-tunnel model of Steptoe Butte area [source position (square) shown with contour lines given in meters above the surrounding ground level

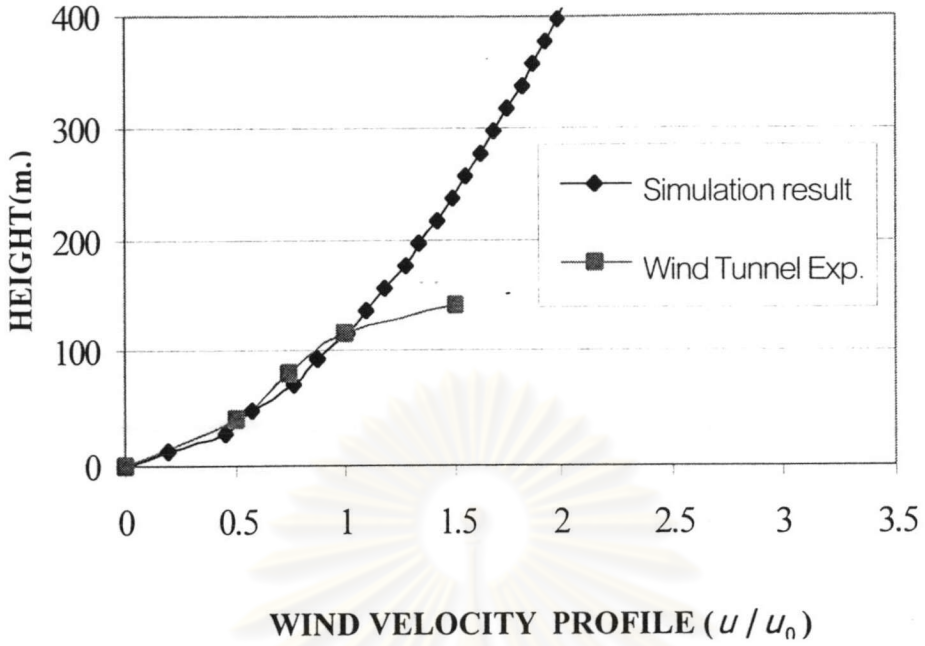

Figure 5.7 Comparison of wind velocity profile between wind tunnel experiment and calculated result.

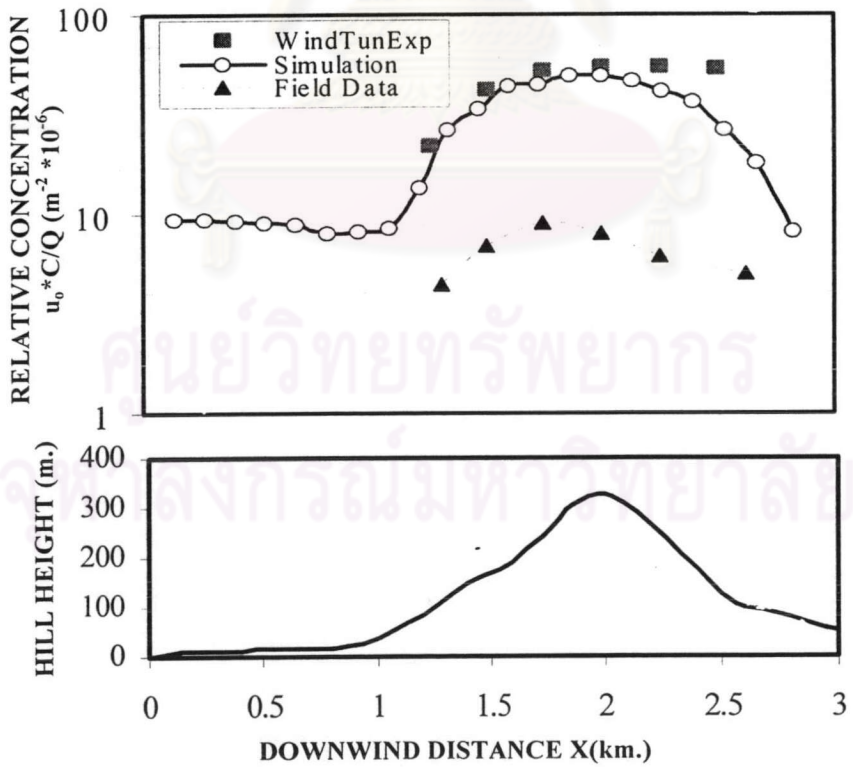

Figure 5.8 Comparison of calculated ground-level downwind concentration with wind tunnel experiment and field test data for wind direction of 192°.

In figure 5.8, the simulation results show that the downwind relative concentration at 10-m height above the ground dramatically increases with the downwind distance up to 2 km. where it agrees well with the wind tunnel experiment. On the other hand, the calculated downwind relative concentration at the same height decrease as the downwind distance increases on the lee side of the hill whereas that of wind tunnel experiment remains more or less the same as the summit value. The reason is that in moderately stable condition, the simulated plume can not readily flow over the hill and travel mainly about the hill, so the calculated concentration on the lee side tends to be lower than the wind-tunnel value. Another cause of the discrepancy may be the assumption of zero concentration at the downwind boundary of the simulation region. When comparing the calculated results with the field test data (B. Lamb,1984) , the calculated concentration gives the same trend as the field test data, but the model over-predicts the concentration because it does not take into account the fact that the wind speed and direction do fluctuate with time during the field test but these time-varying features are difficult to incorporate in the simulation. As a result, all of the field test values are more diluted and lower than those of the calculation. A similar discrepancy exists between the wind-tunnel and field-test data.

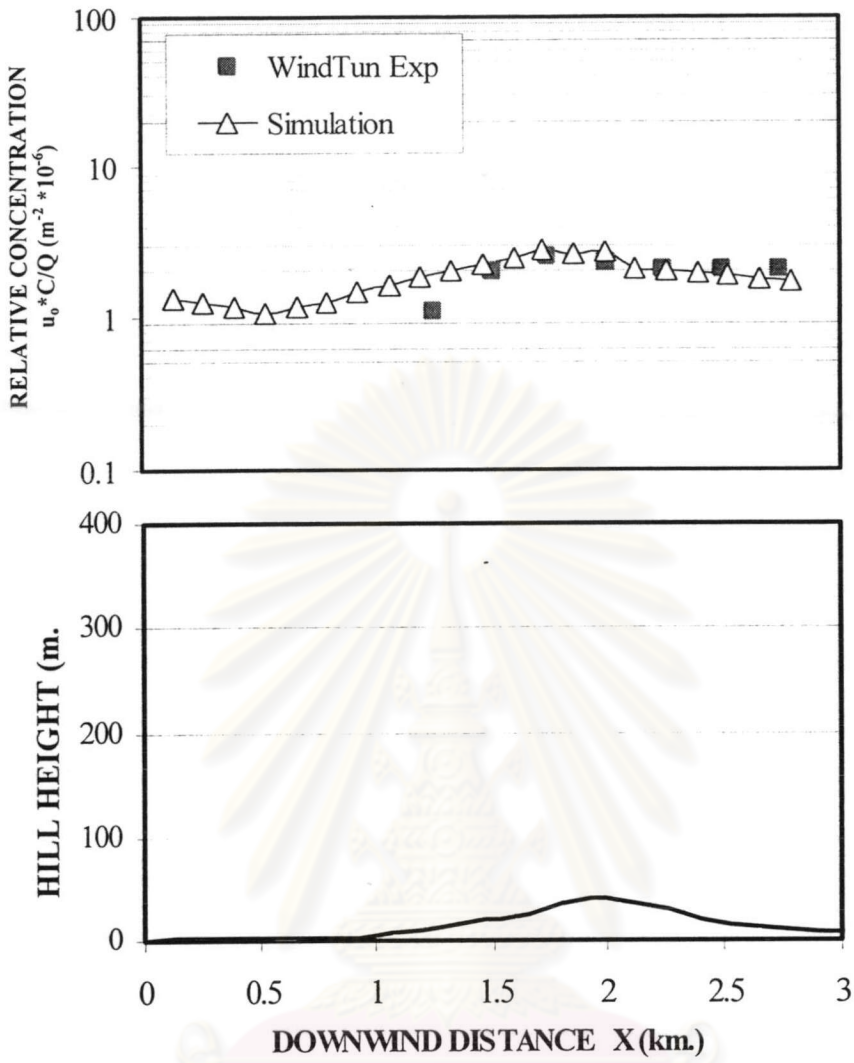

Figure 5.9 Comparison of calculated ground-level downwind concentration with wind tunnel experiment for wind direction of 228°.

In Figure 5.9, the downwind concentration in the case of the wind direction of 228° is found to agree well with the wind tunnel experiment. The calculated relative concentration starts to increase at about 1 km, then begins to decrease slightly at about 2 km. Due to nearly flat topography, the downwind relative concentration remains rather steady. In short, it can be concluded that the present CFD model is highly applicable to the prediction the pollutant concentration over relatively flat topography.

In the next chapter the effects of the various model parameters on the downwind ground-level concentration will be investigated in more detail. As

shown in Figure 5.10 to Figure 5.12, it is clear that, in the case of wind direction of 192 degrees from the north, the effect of the horizontal dispersion coefficient and the vertical dispersion coefficient on the downwind ground-level concentration is more significant than the Reynolds number. The Reynolds number of 1.77×10^{8} is calculated from $\mathrm{Re} = \frac{\rho U_0 h}{\mu}$, where free-stream mean velocity (U_0) = 8.3 m/s, the hill height (h) = 335 m, and the air density and air viscosity at atmospheric pressure and temperature of 11°C are 1.112 kg/m^3 and 1.75×10^{-5} Pa* s, respectively. Similarly, the Reynolds number of 5.27×10^{8} is calculated from $\mathrm{Re} = \frac{\rho U_0 h}{\mu}$, where free-stream mean velocity (U_0) = 8.3 m/s, the height of simulation area (h) = 1,000 m, and the air density and air viscosity at atmospheric pressure and temperature of 11°C are 1.112 kg/m^3 and 1.75×10^{-5} Pa* s, respectively. As expected, in Figure 5.10 the Reynolds number by itself has little influence on the ground-level concentration. The reason is that the present equation of motion do not incorporate any turbulent effect or Reynolds stress terms. Consequently, the change in the Reynolds number has an insignificant effect on the ground-level concentration. In fact, even at the summit, a large increase in the Reynolds number in the model does not affect the wind profile near the ground level, as shown in Figure 5.14. Though not shown here, the effect of Reynolds number on the wind profile at a point on a relatively flat terrain has been found to be negligible.

The horizontal dispersion coefficient positively affect the downwind ground-level concentration, whereas an increase in the vertical dispersion coefficient increases the downwind ground-level concentration from the downwind distance of 0 km. to about 1 km and then decreases the downwind ground-level concentration from the downwind distance of about 1 km. to 3 km. The reason is that the receptor height is much lower than the source height, so in the vicinity of the source a higher vertical dispersion coefficient widens the plume angle sufficiently to reach the nearby ground level. In contrast, at a

distance of 1-3 km not only the effective receptor height was lifted by the topographical elevation but a smaller the plume angle is sufficient. Therefore the downwind ground-level concentration for case of the lower vertical dispersion coefficient becomes higher than that for the case of higher vertical dispersion coefficient because the latter results in more dilution of the downwind ground-level concentration. In Figure 5.13 the exponent of the power law only slightly affects the ground-level concentration. This is because the power-law exponent directly only determines the wind profiles at the upwind and downwind boundaries. As for the wind direction of 228 degree from the north, the effects of these parameters are shown in Appendix A. The effect of these parameters of the model on the predicted concentration at various receptor points will be investigated in the next chapter.

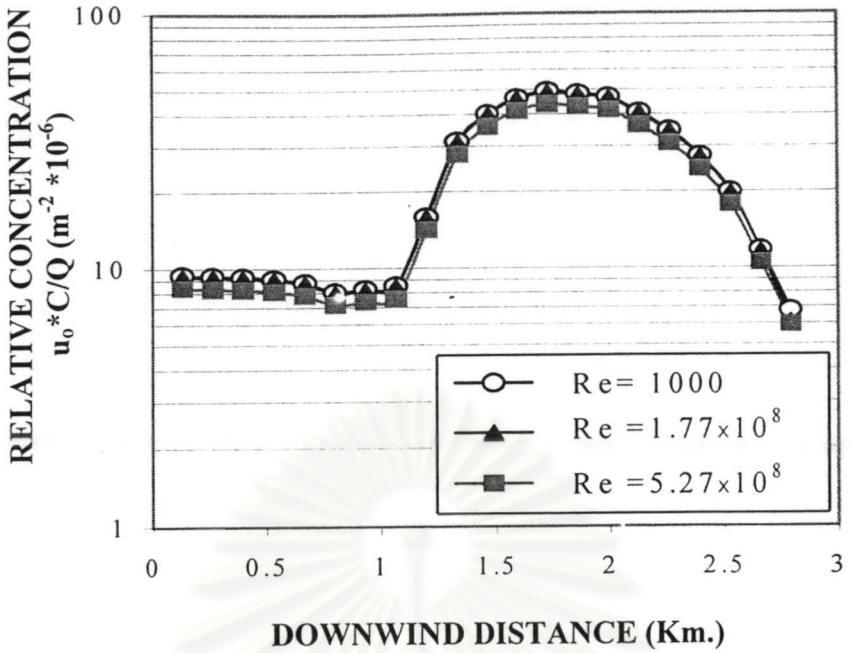

Figure 5.10 Downwind ground-level concentration for wind direction of 192 degrees and various Reynolds numbers with K_H=200 m^2/s, K_V=1 m^2/s, exponent of the power law=0.55

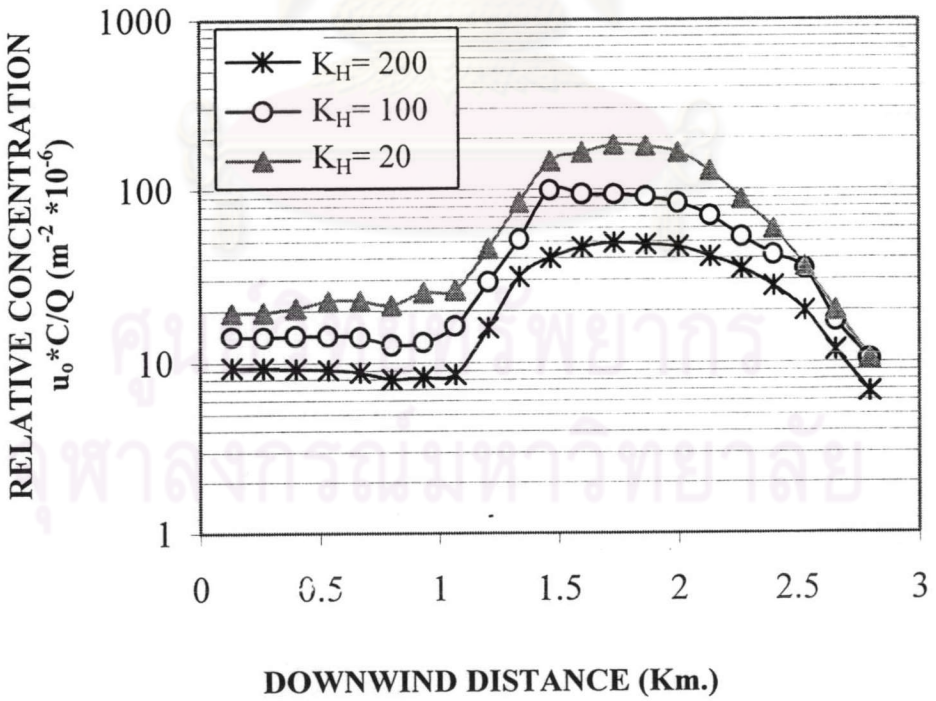

Figure 5.11 Downwind ground-level concentration for wind direction of 192 degrees and various horizontal dispersion coefficients with Re=1000, K_V=1 m^2/s, exponent of the power law=0.55.

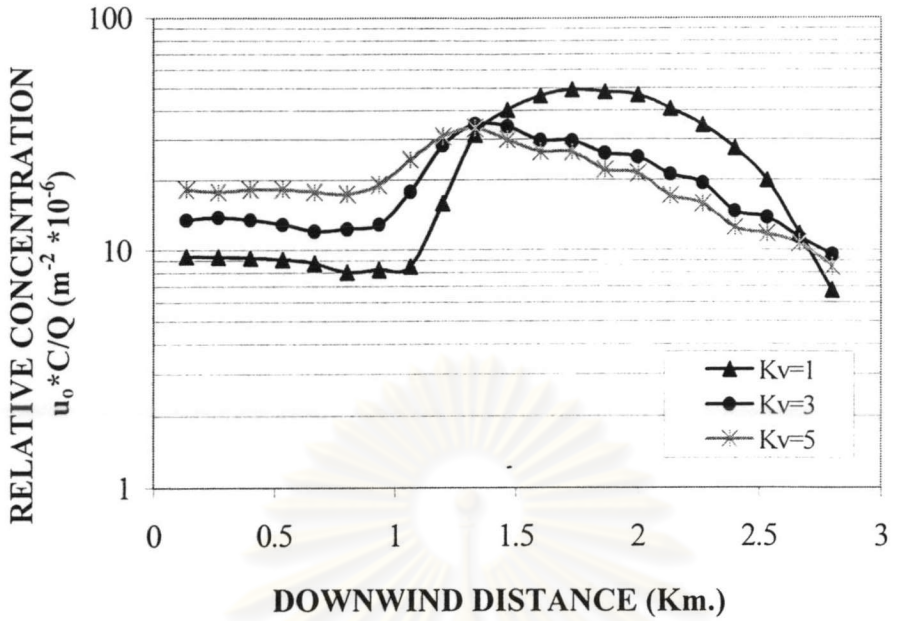

Figure 5.12 Downwind ground-level concentration for wind direction of 192 degrees and various vertical dispersion coefficients with Re=1000, K_H=200 m^2/s, exponent of the power law=0.55.

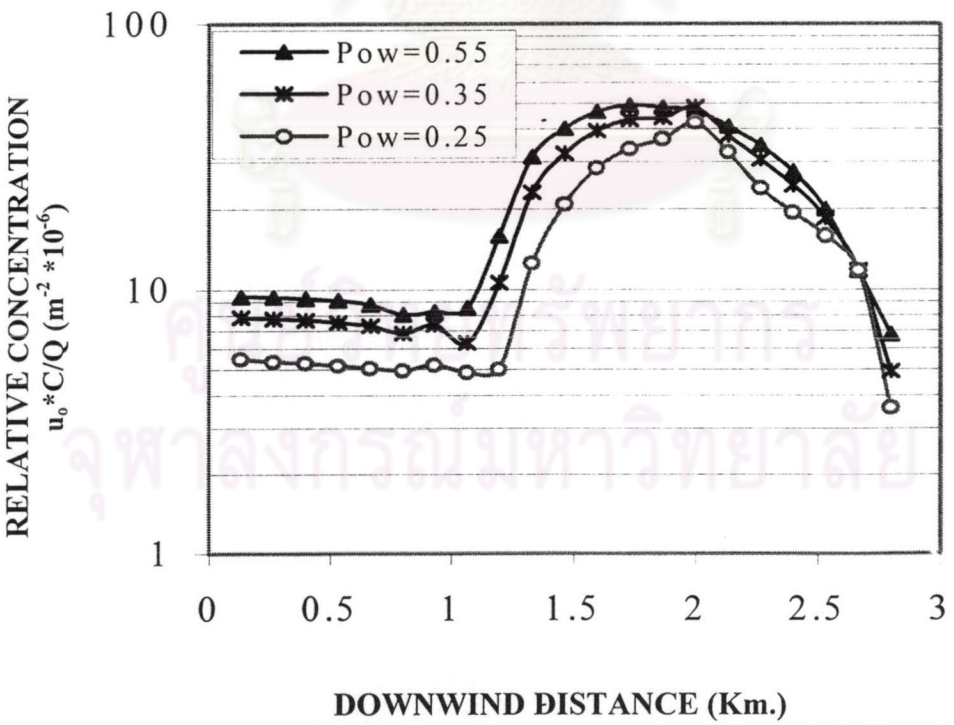

Figure 5.13 Downwind ground-level concentrations for wind direction of 192 degrees and various exponents of the power law with Re=1000, K_H=200 m^2/s, K_v=1 m^2/s

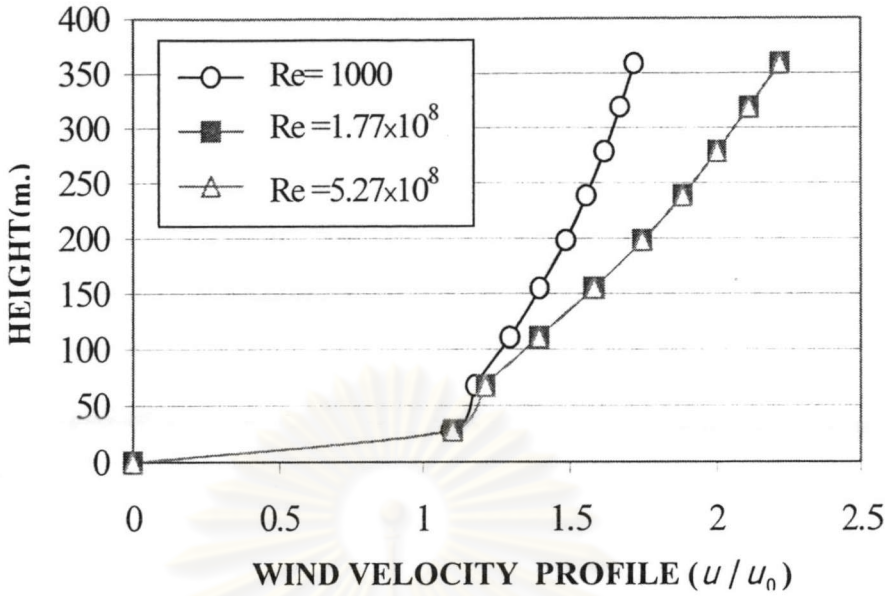

Figure 5.14 Local wind profile at the summit for various Reynolds no. with the exponent of the power law (Pow) =0.55

5.3 Sensitivity to downwind boundary condition

To prove that the choice of downwind boundary condition (B.C.) previous simulations is appropriate, the simulation results from the previous section are compared with those obtain with a change in the boundary condition.

In case of unchanged B.C., boundary condition in horizontal plain as follows:

- $C = 0$, at plane $x = -\frac{\Delta x}{2}$ ($0<z<z_{max}$, $0<y<y_{max}$)
- $C = 0$, at plane $x = x_{max} + \frac{\Delta x}{2}$ ($0<z<z_{max}$, $0<y<y_{max}$)
- $C = 0$, at plane $z = -\frac{\Delta z}{2}$ ($0<x<x_{max}$, $0<y<y_{max}$)
- $C = 0$, at plane $z = z_{max} + \frac{\Delta z}{2}$ ($0<x<x_{max}$, $0<y<y_{max}$)
- $C = 0$, at plane $y = -\frac{\Delta y}{2}$ ($0<x<x_{max}$, $0<z<z_{max}$)
- $C = 0$, at plane $y = y_{max} + \frac{\Delta y}{2}$ ($0<x<x_{max}$, $0<z<z_{max}$)

In case of changed downwind B.C., the boundary conditions are as follows:

- $C = 0$, at plane $x = -\frac{\Delta x}{2}$ ($0<z<z_{max}$, $0<y<y_{max}$)
- $\left(\frac{\partial C}{\partial x}\right)_{z,y} = 0$, at plane $x = x_{max}$ ($0<z<z_{max}$, $0<y<y_{max}$)
- $C = 0$, at plane $z = -\frac{\Delta z}{2}$ ($0<x<x_{max}$, $0<y<y_{max}$)
- $\left(\frac{\partial C}{\partial z}\right)_{x,y} = 0$, at plane $z = z_{max}$ ($0<x<x_{max}$, $0<y<y_{max}$)
- $C = 0$, at plane $y = -\frac{\Delta y}{2}$ ($0<x<x_{max}$, $0<z<z_{max}$)

- $\left(\frac{\partial C}{\partial y}\right)_{x,z} = 0$, at plane $y = y_{max} + \frac{\Delta y}{2}$ ($0<x<x_{max}$, $0<z<z_{max}$)

where C = concentration ($\mu g/m^3$)

From Figure 5.15 and 5.16, the simulation results for the changed boundary conditions slightly better fitted the experimental results than those for the unchanged boundary conditions. According to the zero concentration setting at x_{max} and z_{max}, the downwind concentration near the downwind distance of 3 km inevitably drops in the case of the unchanged boundary conditions. Nevertheless, there is no significant difference between both cases. Figures 5.17 to 5.20 show that the effects of the Reynolds number, the exponent of power law, the horizontal and vertical dispersion coefficients for the changed boundary condition are very similar to those for the unchanged boundary conditions. As expected, the downwind concentration near the end of the horizontal distance for the changed boundary conditions always slightly higher than its counterpart for the unchanged boundary conditions.

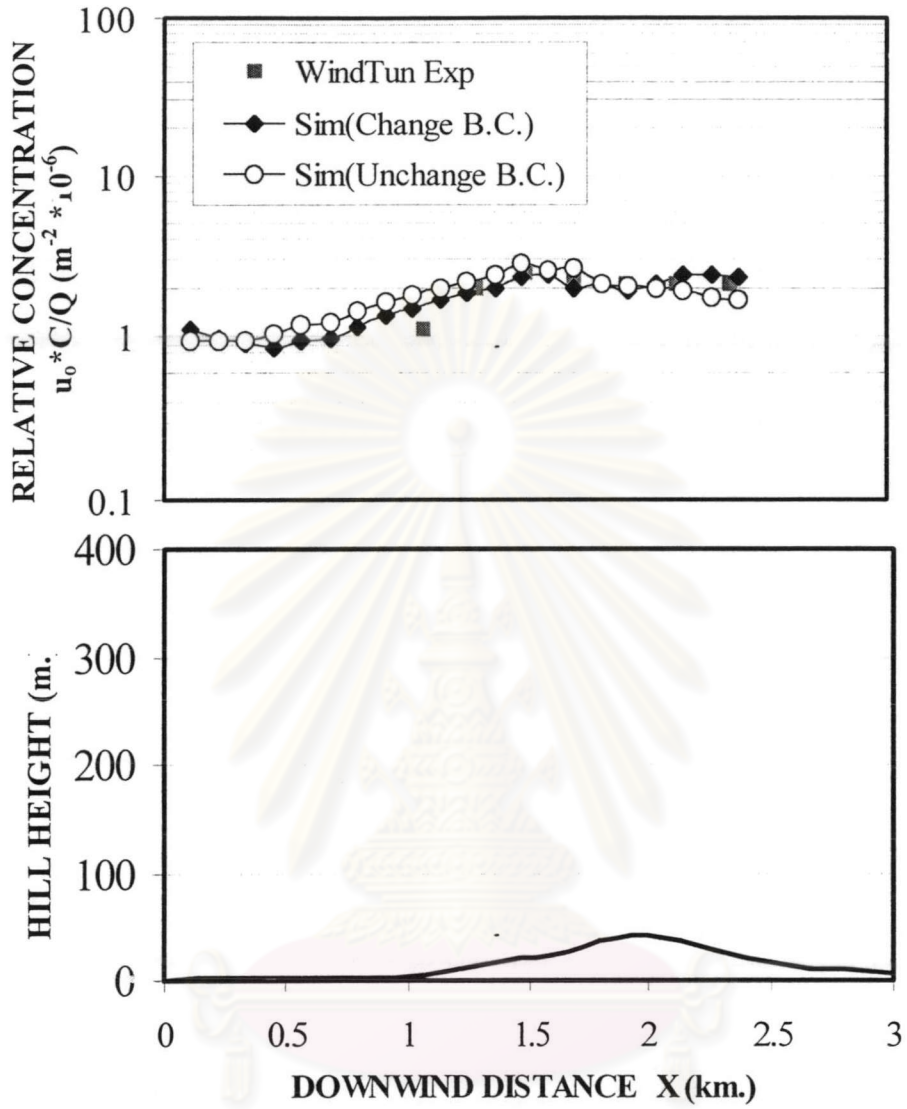

Figure 5.16 Comparison of ground-level downwind concentrations between the changed B.C. and unchanged B.C.for wind direction of 228°.

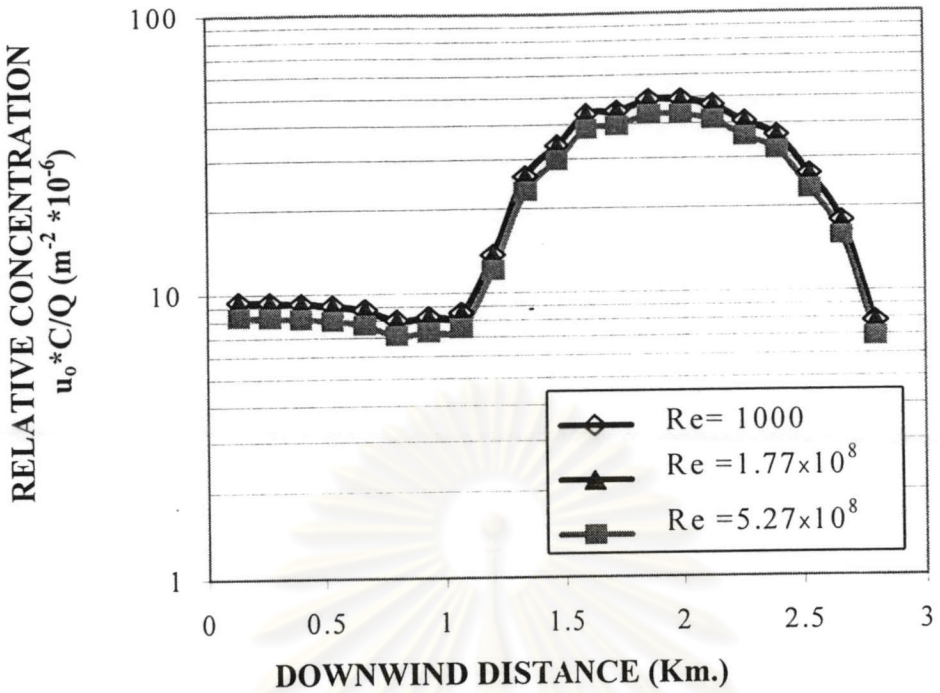

Figure 5.17 Downwind ground-level concentration for wind direction of 192 degrees and various Reynolds numbers with K_H=200 m^2/s, K_v=1 m^2/s, exponent of the power law=0.55 (changed B.C.)

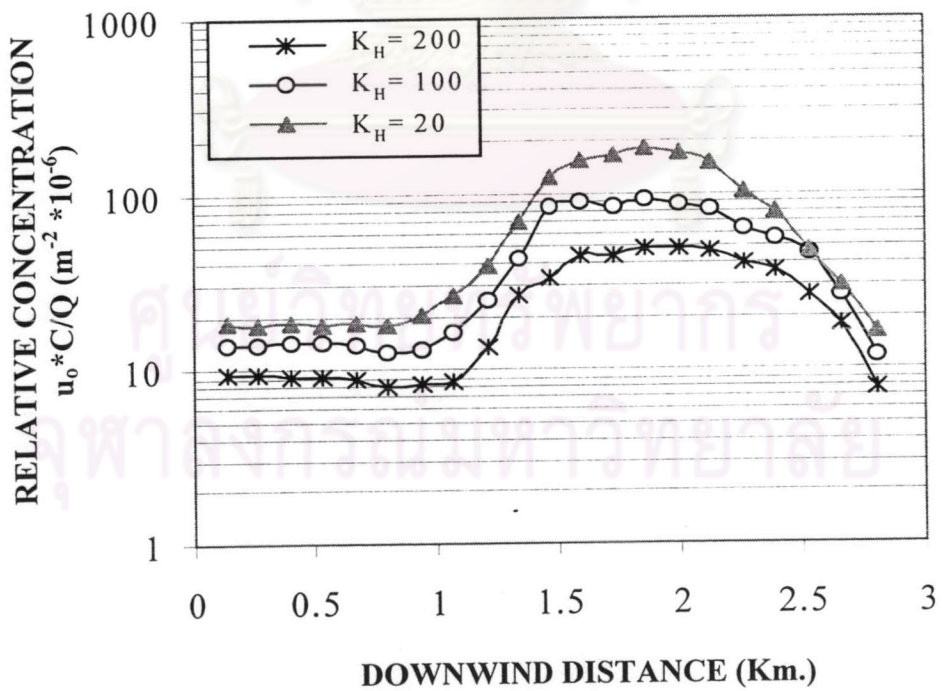

Figure 5.18 Downwind ground-level concentration for wind direction of 192 degrees and various horizontal dispersion coefficients with Re=1000, K_v=1 m^2/s, exponent of the power law=0.55 (changed B.C.)

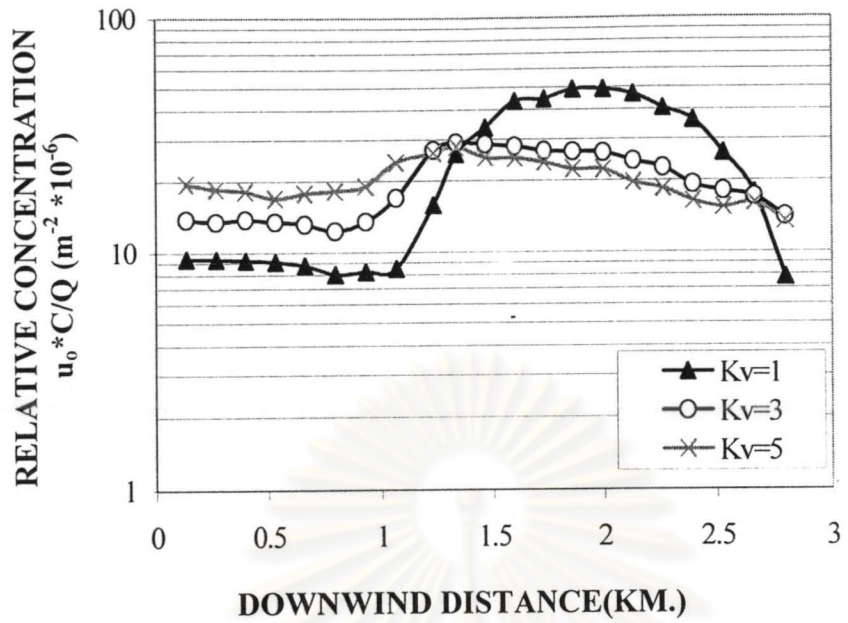

Figure 5.19 Downwind ground-level concentration for wind direction of 192 degrees and various vertical dispersion coefficients with Re=1000, K_H=200 m^2/s, exponent of the power law=0.55 (changed B.C.)

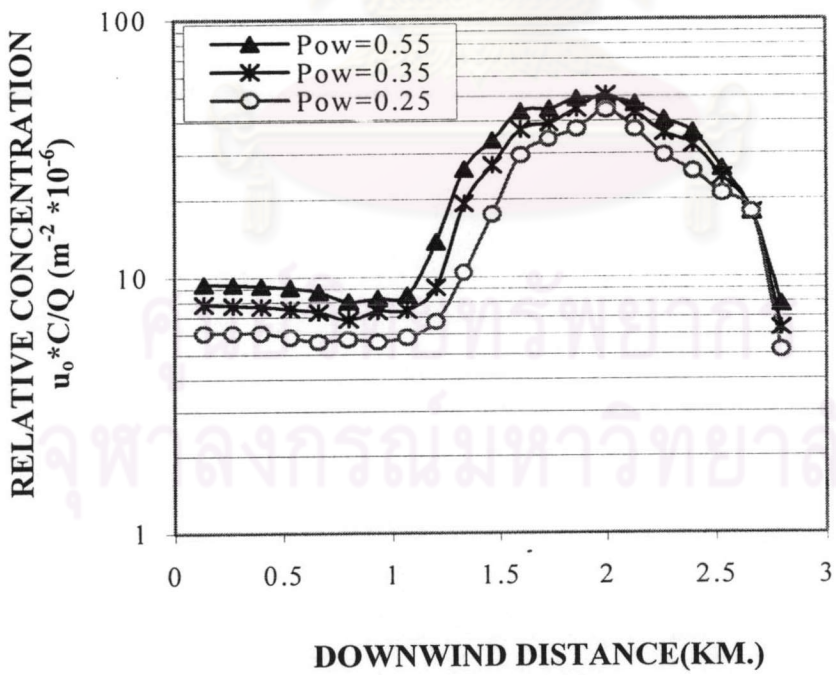

Figure 5.20 Downwind ground-level concentrations of wind direction of 192 degrees and various exponents of the power law with Re=1000, K_H=200 m^2/s, K_v=1 m^2/s (changed B.C.)